Author's Accepted Manuscript

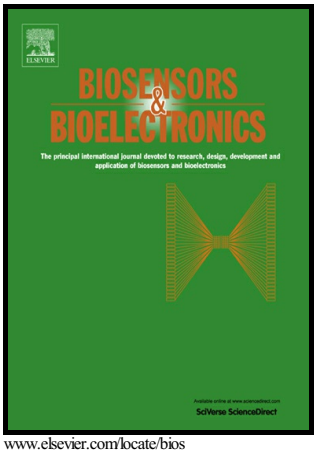

www.elsevier.com/locate/bios

An ultrasensitive biosensor for superoxide anion based on hollow porous PtAg nanospheres

Hongxiao Yang, Jiagang Hou, Zhaohui Wang, Tingting Zhang, Caixia Xu

PII: S0956-5663(18)30467-6
DOI: https://doi.org/10.1016/j.bios.2018.06.034
Reference: BIOS10554

To appear in: *Biosensors and Bioelectronic*

Received date: 23 April 2018
Revised date: 19 June 2018
Accepted date: 19 June 2018

Cite this article as: Hongxiao Yang, Jiagang Hou, Zhaohui Wang, Tingting Zhang and Caixia Xu, An ultrasensitive biosensor for superoxide anion based on hollow porous PtAg nanospheres, *Biosensors and Bioelectronic,* https://doi.org/10.1016/j.bios.2018.06.034

An ultrasensitive biosensor for superoxide anion based on hollow porous PtAg nanospheres

Hongxiao Yang,[a] Jiagang Hou,[b] Zhaohui Wang,[a] Tingting Zhang,[a] and Caixia Xu[a*]

[a] *Institute for Advanced Interdisciplinary Research, School of Chemistry and Chemical Engineering, Jinan 250022, Shandong Province, China*

[b] *Qilu University of Technology (Shandong Academy of Sciences), Jinan 250353, Shandong Province, China*

Fax: +86-531-82767046; Tel: +86-531-82767046

*Email: chm_xucx@ujn.edu.cn (C. Xu)

ABSTRACT

The accurate detection of the superoxide anion ($O_2^{\bullet-}$) has vital academic and medical diagnostic significance due to its important dual roles in biological functioning. In this work, hollow porous PtAg nanospheres (PtAg HPNSs) were fabricated by a facile hydrothermal method followed by a dealloying procedure. The as-made PtAg nanospheres possessed hollow interiors and porous shells composed of interconnected ligaments and pores with the typical size around 4 nm. Benefitting from the unique hollow nanoporous architecture and the specific alloying effect, the PtAg HPNSs showed

high electrocatalytic activity towards superoxide anions. The constructed biosensor based on PtAg HPNSs presented a fast and ultrasensitive response in a wide range of 0.8 to 1080 nM with much higher sensitivity of 4.5×10^{-2} μA cm^{-2} nM^{-1} and low detection limit of 0.2 nM (S/N=3). Moreover, the novel biosensors can achieve electrochemical detection for $O_2^{\bullet-}$ released from living cells, exhibiting outstanding real time detection capability in cell environment. The facile controllable fabrication and unique sensing performance for PtAg HPNSs offers potential practical applications in developing highly sensitive and stable biosensor towards superoxide anion.

Keywords: platinum; hollow; porous; electrochemical biosensor; superoxide anion

1. Introduction

Reactive oxygen species, including hydroxyl radicals, superoxide radicals, and hydrogen peroxide, are involved in various physiological and pathological processes (Tang et al., 2015; Madhurantakam et al., 2014). Superoxide anion ($O_2^{\bullet-}$), a product of the metabolic reactions, holds a special place in the organism functioning (Hayyan et al., 2016), which mainly generate from the mitochondrial respiratory chain and phagocytic nicotinamide adenine dinucleotide phosphate oxidase. $O_2^{\bullet-}$ not only serves as a regulatory mediator in signaling and immune processes under normal physiological conditions, but

also plays an important role in the occurrence of certain diseases by causing oxidative damage to DNA, protein, and biological membranes when excessive $O_2^{\bullet-}$ accumulates (Wang et al., 2017a). Therefore, the quantification of $O_2^{\bullet-}$ can act as a risk indicator for many oxidative stress-induced diseases including Parkinson's disease, cancer, Alzheimer's disease, autoimmune diseases as well as aging et al. (Madhurantakam et al., 2014; Hayyan et al., 2016). Thus, the sensitive, selective, reliable, and quick detection of $O_2^{\bullet-}$ is urgently required for the clinical pathological diagnosis and health screening.

Up to date, many methods have been developed to detect $O_2^{\bullet-}$, such as fluorescence (Jang et al., 2014; Song et al., 2017; Xiao et al., 2017), electron spin resonance (Wang et al., 2013; Bézière et al., 2010), chromatography (Wang et al., 2015), and electrochemical technique (Wang et al., 2016; Liu et al., 2017a; Liu et al., 2017b). Among these assays, the electrochemical method has received extensive attentions due to the advantages of excellent sensitivity, high accuracy, superior portability, easy operation, as well as effective detection of the target species (Liu et al., 2017c; Braik et al., 2016). Although the electrochemical sensors based on the immobilization of enzymes onto functionalized electrodes, such as superoxide dismutase (SOD), present good selectivity and sensitivity (Zhu et al., 2015; Thandavan et al., 2013), the high dependence on the external conditions (pH, temperature, and humidity et al.), the short lifetime, poor structural stability, and relatively high cost of enzyme-based biosensor restrict its practical applications (Liu et al., 2017a). Considerable efforts have been dedicated to explore the enzyme-free electrochemical $O_2^{\bullet-}$ sensors in view of the high catalytic activity over various nanomaterials (Wei et al., 2018; Kim et al., 2012). Platinum has been found to possess superior SOD enzyme-like activity with the intrinsic advantages of fast electron transport,

excellent electrocatalytic activity, impressive electrochemical stability, and broad environmental suitability (Hu et al., 2013; Kajita et al., 2007; Hamasaki et al., 2008; Kim et al., 2012). Nevertheless, the monometallic Pt is susceptible to the poisoning from absorbed intermediates, while the catalytic performance is easily affected by some natural antioxidants, such as ascorbic acid, dopamine, and uric acid (Park et al., 2003; Bo et al., 2010). It is noted that the alloying strategy by introducing the other transition metals to Pt can effectively alleviate these problems due to the preferable synergistic effects compared with the single counterparts (Liu et al., 2015; Chen et al., 2012). For example, Hu et al. reported that the SOD enzyme-like activity of Au@Pt nanorods can be tailored via alloying with Ag due to the large modification of the electronic structure (Hu et al., 2013). Ren et al. constructed a nonenzymatic electrochemical sensor based on PtRuCu ternary alloy with a linear range of 7.5-330 μM and detection limit of 0.7 μM, which is considered to result from the fast electron transfer rate and enhanced electrocatalytic performance over the Pt-based alloy (Ren et al., 2017).

The sensing performances can be optimized by engineering the structure and morphology of the nanomaterials related to the enhancement of electrochemical active sites as well as the fluent mass transfer (Sadeghian et al., 2017). Among a variety of nanoscaled materials, hollow structures are preferable with the advantages of high specific surface area and saving of material. With the concerns above, hollow PtAg nanospheres with nanoporous shell were designed and prepared via a facile hydrothermal method followed by a dealloying strategy in this work. The as-made PtAg alloy HPNSs is particularly desirable for electrochemical sensing with open pores, inner and outer porous surface, and interconnected small grains on the shell. Moreover, the hollow porous

structure is beneficial for the reaction medium contact with more active sites through nanoporous internal and external surface. In addition, the integrated interconnected network backbone and abundant pores can promote the unlimited electron and mass transport during electrochemical catalysis (Zhu et al., 2016; Qiu et al., 2014). The as-constructed biosensors based on PtAg HPNSs exhibited outstanding sensing performance towards $O_2^{\bullet-}$ with a wide linear range, low detection limit, and excellent sensing stability. Importantly, the developed PtAg biosensors present excellent real time detection of $O_2^{\bullet-}$ released from HeLa and Raw 264.7 cells, offering a great feasibility for widespread applications in clinic diagnostics.

2. Experimental

2.1. Reagents and apparatus

18-crown-6, potassium dioxide (KO_2), and chloroplatinic acid hexahydrate (H_2PtCl_6) were purchased from Aladdin Industrial Inc. Dimethyl sulphoxide (DMSO), silver nitrate ($AgNO_3$), Polyvinylpyrrolidone (PVP), ammonia solution ($NH_3.H_2O$), glucose, and ethanol were purchased from Sinopharm Chemical Reagent Co. Ltd. The commercial John-Matthey Pt/C catalyst (20 wt.%) was purchased from Alfa Aesar. Ascorbic acid (AA), dopamine (DA), and uric acid (UA) were purchased from Sigma-Aldrich. Zymosan was purchased from Macklin. The phosphate buffered saline (0.1 M PBS, pH 7.4) solution was prepared using Na_2HPO_4 and KH_2PO_4. All chemicals were of analytical grade and used without further purification. Ultra-pure water (18.2 MΩ cm) was used throughout the whole operation process.

The X-ray diffraction (XRD) analysis was performed on a Bruker D8 advanced X-ray diffractometer using Cu Kα radiation at a step rate of 0.04° s^{-1}. The microstructure and

composition of the samples were characterized using a transmission electron microscope (TEM, JEM-2100) and a field-emission scanning electron microscope (FE-SEM, JSM-6700). High-resolution TEM (HRTEM) and elemental mapping images were acquired by scanning transmission electron microscopy-energy dispersive X-ray spectroscopy using a JEM 2100F TEM equipped with a STEM unit. All electrochemical measurements were conducted on a CHI 760D electrochemical workstation (Shanghai CH Instruments Co., China). A conventional three-electrode system was used with a 4 mm diameter glassy carbon electrode as the working electrode, Pt foil as the counter electrode, and mercury sulfate electrode as the reference electrode.

2.2. Preparation of PtAg HPNSs

The PtAg HPNSs was prepared by a modified method as reported in references (Gu et al., 2009; Fan et al., 2015). In a typical procedure, after 0.35 g PVP and 0.1 g $AgNO_3$ dissolved in 8 ml ethylene glycol, 2 ml $H_2PtCl_6.2H_2O$ in ethylene glycol solution (0.03 g ml^{-1}) was added to the mixture under vigorous stirring, followed by the addition of 100 μL $NH_3.H_2O$. Then the homogeneous solution was transferred into a Teflon-lined autoclave of 20 mL capacity and heated for 4 h at 200 $^{\circ}C$. After the autoclave was cooled to room temperature naturally, the precursor was centrifuged and washed 3 times with deionized water and absolute ethanol sequentially. The final PtAg sample was obtained by etching the precursor in HNO_3 (~14 M) solution for 15 min at room temperature and washed several times with water.

2.3. Generation of superoxide anion

The stock solution of $O_2^{\bullet-}$ was prepared by dissolving KO_2 in DMSO solution with 18-crown-6, which was stored together with 4 Å molecular sieves to remove traces of H_2O.

According to the molar absorptivity of $O_2^{\bullet-}$ in DMSO (2006 M^{-1} cm^{-1} at 271 nm), the concentration of $O_2^{\bullet-}$ could be estimated by a UV-Vis spectroscope (Liu et al. 2017c; Zhu et al. 2016).

2.4. Preparation of the modified electrodes

Catalyst ink was prepared by sonicating the mixture of 1.0 mg PtAg alloy powder, 400 μL isopropanol, 200 μL Nafion solution (0.5 wt.%), and 1.0 mg carbon powder for 30 min to form uniform suspension solution. The working electrode was made by placing appropriate catalyst ink on a polished glassy carbon electrode (GCE, 4 mm in diameter) and dried. The Pt/C modified electrodes were prepared in a similar way. All potentials were provided according to the reversible hydrogen electrode (RHE) scale for clarity. The electrochemical active surface area of Pt-based catalysts were calculated by integrating the reduction charges during the stripping of surface monolayer oxide in N_2-purged 0.5 M H_2SO_4 solution in the range of 0 to 1.35 V at the scan rate of 50 mV s^{-1}, in which the used charge density is 210 μC.cm^{-2} Pt (Zhan et al. 2009; Xu et al. 2013).

2.5. Cell culture and real time monitoring of superoxide anion from living cell

The Raw 264.7 cells and HeLa cells were cultured in culture vessels containing Dulbecco's modified Eagle's medium medium, 10% fetal bovine serum, and 1% penicillin/streptomycin. These two cell lines were maintained in a humid incubator with an atmosphere consisted of 95% air and 5% CO_2 at 37 °C. The number of cells was counted through a microscopy and was calculated to be 1.0×10^7. All the cells were collected through centrifugation (1000 rpm, 5 min) and dispersed in 8 mL PBS for the real time electrochemical measurements. The experiments were conducted in the water

bath at 37 °C.

3. Results and discussion

3.1. Characterization of the PtAg HPNSs

Fig. 1a presents the SEM image of the as-made PtAg alloy sample, from which one can distinguish the spherical nanostructure with the diameter mainly distributed around 50 nm. The detailed structure was further characterized by TEM. From Fig. 1b, the obvious brightness contrast between the dark shell and the relatively light region reveals the hollow nature of the obtained PtAg nanospheres. The high magnification TEM image in Fig. 1c indicated that the hollow PtAg spheres are composed of interconnected ligaments and pores with the shell thickness around 5 nm. Fig. 1d gives the corresponding HRTEM image, where the pores uniformly penetrated on the shell with the typical ligament size around 4 nm. The highly ordered lattice fringes with a period of 0.234 nm can be well indexed to the (111) crystal plane of face-centered cubic structure of PtAg alloy (Yousaf et al. 2016; Lv et al. 2014b). It is clear that the as-made PtAg alloy possesses high porosity and bicontinuous nanoscaled backbone with the narrow ligament sizes as small as 4 nm. As depicted in Fig.1e-g, the elemental mappings clearly show the uniform distribution of Pt and Ag elements throughout the entire nanostructure, demonstrating the successful formation of uniform PtAg HPNSs.

The crystal structure of PtAg HPNSs was characterized by XRD with the standard diffraction patterns of pure Pt and Ag metals provided for comparison. As depicted in Fig. 2a, the diffraction pattern of PtAg alloy exhibits only one set of three diffraction peaks locating around 38.6, 45.2, and 65.2, which can be indexed to (111), (200), and (220) crystal planes for a face-centered-cubic (fcc) PtAg alloy (Zheng et al. 2016; Lv et al.

2014a). The three peaks located just between standard diffraction peaks of pure Pt and Ag with no peaks assigned to pure Pt, Ag, or any oxides appeared, revealing the formation of a homogeneous single-phase PtAg alloy (Cao et al. 2015). X-ray energy-dispersive spectroscopy (EDS) (Fig. 2b) reveals that its composition is $Pt_{57}Ag_{43}$ (at.%).

3.2. Electrochemical sensing of $O_2^{\bullet-}$ over PtAg HPNSs

The PtAg HPNSs represent one class of advanced nanoarchitecture, which is beneficial for the unlimited mass transport and high electron conductivity during the electrocatalytic process. The electrocatalytic behaviors of PtAg HPNSs toward $O_2^{\bullet-}$ were investigated by cyclic voltammetric method (CV) to evaluate its potential application in $O_2^{\bullet-}$ sensing. Fig. 3 shows the CV profile of PtAg HPNSs in the absence and presence of $O_2^{\bullet-}$ (Fig. 3a) with that of commercial Pt/C and bare GCE modified electrodes provided for comparison (Fig. 3b&c). It is noted that there are only weak current responses after the addition of $O_2^{\bullet-}$ over the bare GCE and Pt/C modified electrode. By comparison, the significantly improved oxidation signals in a wide potential range starting from 0.6 V was observed for PtAg HPNSs, suggesting its superior electrocatalytic activity towards $O_2^{\bullet-}$ oxidation.

The electrocatalytic behaviour of PtAg HPNSs toward $O_2^{\bullet-}$ oxidation was further explored by changing the scan rate from 10 mV s^{-1} to 100 mV s^{-1}. Fig. S1a shows the CV curves of the PtAg HPNSs recorded in the presence of 0.01 mM $O_2^{\bullet-}$ in PBS solution (pH 7.4). It is clear that the current at 0.9 V is linear as a function of the scan rate in a range from 10 to 100 mV s^{-1} (Fig. S1b), and the corresponding linear equation is j (μA cm^{-2}) = 8.68+1.43 v (R^2=0.998), which demonstrates that the electrochemical oxidation $O_2^{\bullet-}$ over the PtAg HPNSs modified electrode is a surface-controlled process (Madhurantakam et al. 2014; Zhou et al. 2011).

The amperometric detection upon the step-wise addition of $O_2^{\bullet-}$ was carried out to further evaluate the possibility of the PtAg HPNSs as enzyme-free biosensors. Fig. 4a shows the typical current responses of PtAg HPNSs to the successive addition of $O_2^{\bullet-}$ under the constant potential of 0.9 V in the PBS solution. It is clearly observed that once the $O_2^{\bullet-}$ was added, the response currents increases rapidly and reaches the maximum steady-state current within a short period of 2 s. The sensitive and fast response of the PtAg HPNSs may arise from the specific alloy effect and unique hollow nanoporous architecture. The high electric conductivity of the PtAg alloy facilitates the fast electron transfer during the process of electrochemical oxidation of $O_2^{\bullet-}$. The voids and channels in the hollow porous architecture provide smooth mass transport pathway to shorten the response time. Besides, the large surface area of hollow porous structure provides abundant electrochemical active sites to enhance the sensing sensitivity (Liu et al. 2017a).

In addition, the corresponding calibration curve was presented in Fig. 4b. A linear response for $O_2^{\bullet-}$ was acquired from 0.8 to 1080 nM (linear equation: j (μA cm^{-2}) = 0.065+0.045 $c(O_2^{\bullet-})$, R^2=0.999), with the limit of detection (LOD) as 0.2 nM based on a signal to noise (S/N=3). The sensitivity is determined to be as high as 0.045 μA cm^{-2} nM^{-1}. Furthermore, the sensing performances of the as-constructed sensor were compared with the previous reports in Table S1 (Liu et al., 2017a, Zhu et al., 2015; Thandavan et al., 2013; Ren et al., 2017; Wang et al., 2017b; Tang et al., 2015; Wang et al., 2018). It illustrates that the PtAg HPNSs based biosensors in this work shows much better sensitivity and lower detection limit in the certain concentration range.

3.3. The selectivity, reproducibility, and stability for $O_2^{\bullet-}$ detection over PtAg HPNSs

The selectivity, reproducibility, and stability are also the important parameters to

evaluate the sensing performance for electrochemical biosensors. One of the main challenges in the electrochemical detection of $O_2^{\bullet-}$ is the interfering electrochemical signals caused by some compounds, such as AA, UA, DA, glucose, and ethanol, which are possibly oxidized along with $O_2^{\bullet-}$ on the electrode surface (Park et al. 2003; Bo et al. 2010; Peng et al. 2017). To explore the selectivity of PtAg HPNSs toward the $O_2^{\bullet-}$ sensing, the amperometric responses were monitored for the modified electrode upon the addition of these electroactive species into the electrolyte. Fig. 5a shows the current responses to the successive addition of 0.5 mM AA, 0.5 mM UA, 0.5 mM DA, 5 mM glucose, 1 mM ethanol, and 1.0 μM $O_2^{\bullet-}$ in a stirred PBS solution at 0.9 V. No noticeable interference from AA, UA, DA, glucose, and ethanol was observed in related to the response generated by $O_2^{\bullet-}$, suggesting that PtAg HPNSs are favorable to construct the enzyme-free biosensors towards $O_2^{\bullet-}$ with excellent selectivity and high anti-interference performance.

The reproducibility of the developed sensor was tested using five different electrodes at the same condition. The relative standard deviations of the current responses were less than 2.0% (Fig. 5b). Moreover, the long-term catalytic stability of PtAg HPNSs was also carried out by detecting the steady-state specific activity using the potentiostatic method. Fig. 5c presents the chronoamperometry data of 1.0 μM and 5.0 μM $O_2^{\bullet-}$ in stirring PBS solutions under 0.9 V. It is noted that 96.6% of the initial current was maintained with 5.0 μM $O_2^{\bullet-}$ after continuously running for 4000 s, while 87.4% was remained in 1.0 μM $O_2^{\bullet-}$ solution. The relatively lower sensing stability in 1.0 μM $O_2^{\bullet-}$ solution may result from the low concentration of $O_2^{\bullet-}$. The PtAg HPNSs could promote the oxidation of $O_2^{\bullet-}$ into H_2O. As the oxidation proceeds, more and more $O_2^{\bullet-}$ are exhausted with the oxidation

current degraded. The relatively stable amperometric response under the high concentration of $O_2^{\bullet-}$ indicates that PtAg HPNSs have outstanding sensing stability under the enough supply of $O_2^{\bullet-}$. These results above demonstrate that the PtAg HPNSs based sensors possess excellent selectivity, respectable reproducibility, and stability for the practical $O_2^{\bullet-}$ detection.

The superior electrocatalytic activity of PtAg HPNSs toward $O_2^{\bullet-}$ is considered to stem from several factors. First, the hollow porous architecture and integral network nanoshell facilitate the unlimited mass transport and fast electrons transfer during electrocatalysis, which is beneficial for reducing the reaction and diffusion resistance and favoring the electrochemical reaction kinetics (Xu et al. 2011). Second, the full access of the nanoporous internal and external surface can provide the large active surface area to reaction medium with highly efficient usage of the catalyst material (Wang et al., 2017b). In addition, the synergistic catalytic effect by alloying Pt with Ag may dramatically enhance the electrocatalytic activity toward $O_2^{\bullet-}$ oxidation.

3.4 Detection of $O_2^{\bullet-}$ release from living cells

Encouraged by the exciting electrochemical sensing performance above, the constructed biosensor based on PtAg HPNSs was further applied to real time detection for $O_2^{\bullet-}$ in the cellular environment. Raw 264.7 cells and HeLa cells were chosen as the model cells, while zymosan was employed as the functional agent to stimulate living cells to release $O_2^{\bullet-}$ (Wang et al., 2017b). The real time monitoring for $O_2^{\bullet-}$ released from living cells was carried out using chronoamperometry method. The dynamic responses of the Raw 264.7 cells upon the successive injection of 10 mg ml^{-1} Zymosan were presented in Fig. 6a. A significant current increase corresponding to $O_2^{\bullet-}$ oxidation occurred once

Zymosan was injected into the cell suspension. By comparison, the current change was also recorded upon the injection of Zymosan into PBS solution in the absence of Raw 264.7 cells. No obvious current response was observed at each addition of Zymosan at the same condition, demonstrating that the current response in the red curve of Fig. 6a resulted from the Zymosan-induced $O_2^{\bullet-}$ from Raw 264.7 cells.

In addition, the responses of HeLa cells upon the successive injection of Zymosan were also shown in Fig. 6b. Compared with Raw 264.7 cells, the relative weaker response current was obtained, suggesting that less $O_2^{\bullet-}$ was released from HeLa cells under the same Zymosan stimulation. The outstanding capability for real time detection was mainly attributed to the ultrahigh sensitivity of the PtAg HPNSs based biosensors.

4. Conclusions

In current work, hollow porous PtAg nanospheres with integral network nanoshell were successfully prepared via a facile hydrothermal method and dealloying strategy. The constructed biosensors based on PtAg HPNSs show unique sensing performances of high sensitivity, wide linear range, low detection limit, excellent selectivity, good stability towards $O_2^{\bullet-}$ detection. These unique sensing performances mainly originates from the structural superiority of PtAg HPNSs: (1) the fast electron and mass transport in the hollow porous structure from interconnected conductive network and smooth channels, (2) the full access of the large active surface area to reaction medium, (3) robust integrated architecture and alloying effect of the nanostructured PtAg alloy. Inspiringly, real time detection of $O_2^{\bullet-}$ released from two cells lines (HeLa and Raw 264.7 cells) is achieved with the PtAg HPNSs based biosenors, indicating that the proposed biosensors hold promising application prospect in fundamental research and clinic diagnostics.

Acknowledgements

This work was supported by the National Natural Science Foundation of China [21506072, 51772133] and Shandong Province [ZR2017JL022], and China postdoctoral science foundation [2017M622117].

References

Bézière, N., Frapart, Y., Rockenbauer, A., Boucher, J., Mansuy, D., Peyrot, F., 2010. Metabolic stability of superoxide and hydroxyl radical adducts of a cyclic nitrone toward rat liver microsomes and cytosol: A stopped-flow ESR spectroscopy study. Free Radic. Biol. Med. 49, 437-446.

Bo, X., Ndamanisha, J.C., Bai, J., Guo, L., 2010. Nonenzymatic amperometric sensor of hydrogen peroxide and glucose based on Pt nanoparticles/ordered mesoporous carbon nanocomposite. Talanta 82, 85-91.

Braik, M., Barsan, M. M., Dridi, C., Alic, M. B., Brett, C.M.A., 2016. Highly sensitive amperometric enzyme biosensor for detection of superoxide based on conducting polymer/CNT modified electrodes and superoxide dismutase. Sens. Actuators B: Chem. 236, 574-582.

Cao, X., Wang, N., Han, Y., Gao, C., Xu, Y., Li, M., Shao, Y., 2015. PtAg bimetallic nanowires: Facile synthesis and their use as excellent electrocatalysts toward low-cost fuel cells. Nano Energy 12, 105-114.

Chen, K.J., Pillai, K. C., Rick, J., Pan, C.J., Wang, S.H., Liu, C.C., Hwang, B.J., 2012. Bimetallic PtM (M=Pd, Ir) nanoparticle decorated multi-walled carbon nanotube enzyme-free, mediator-less amperometric sensor for H_2O_2. Biosens. Bioelectron. 33, 120-127.

Fan, Y., Liu, P., Zhang, Z., Cui, Y., Zhang, Y., 2015. Three-dimensional hierarchical porous platinumecopper alloy networks with enhanced catalytic activity towards methanol and ethanol electro-oxidation. J Power Sources 296, 282-289.

Gu, X., Xu, L., Tian, F., Ding, Y., 2009. Au-Ag alloy nanoporous nanotubes. Nano Res 2, 386-393.

Hamasaki, T., Kashiwagi, T., Imada, T., Nakamichi, N., Aramaki, S., Toh, K., Morisawa, S., Shimakoshi, H., Hisaeda Y., Shirahata, S., 2008. Kinetic analysis of superoxide anion radical-scavenging and hydroxyl radical-scavenging activities of platinum nanoparticles, Langmuir 24, 7354-7364.

Hayyan, M., Hashim, M.A., AlNashef, I.M., 2016. Superoxide ion: generation and chemical implications. Chem. Rev. 116, 3029-3085.

Hu, X., Saran, A., Hou, S., Wen, T., Ji, Y., Liu, W., Zhang, H., He, W., Yin, J., Wu, X., 2013. Au@PtAg core/shell nanorods: tailoring enzyme-like activities via alloying. RSC Adv. 3, 6095-6105.

Jang, Y.J., Murale D.P., Churchill, D.G., 2014. Novel reversible and selective nerve agent simulant detection in conjunction with superoxide “turn-on” probing. Analyst 139, 1614-1617.

Kajita, M., Hikosaka, K., Iitsuka, M., Kanayama, A., Toshima N., Miyamoto, Y., 2007. Platinum nanoparticle is a useful scavenger of superoxide anion and hydrogen peroxide. Free Radical Res. 41, 615-626.

Kim, S.K., Kim, D., You, J.M., Han, H.S., Jeon S., Non-enzymatic superoxide anion radical sensor based on Pt nanoparticles covalently bonded to thiolated MWCNTs, Electrochim. Acta, 2012, 81, 31-36.

Liu, F., Xiang, G., Jiang, D., Zhang, L., Chen, X., Liu, L., Luo, F., Li, Y., Liu, C., Pu, X., 2015. Ultrasensitive strategy based on PtPd nanodendrite/nano-flower-like@GO signal amplification for the detection of long non-coding RNA. Biosens. Bioelectron. 74, 214-221.

Liu, L., Zhao, H., Shi, L., Lan, M., Zhang, H., Yu, C., 2017a. Enzyme- and metal-free electrochemical sensor for highly sensitive superoxide anion detection based on nitrogen doped hollow mesoporous carbon spheres. Electrochim. Acta 227, 69-76.

Liu, Y., Liu, X., Liu, Y., Liu, G., Ding, L., Lu, X., 2017b. Construction of a highly sensitive non-enzymatic sensor for superoxide anion radical detection from living cells. Biosens. Bioelectron. 90, 39-45.

Liu, X., Liu, X., Wei, H., Song, G., Guo, H., Lu, X., 2017c. Sensitive detection of superoxide anion released from living cells using silver nanoparticles and functionalized multiwalled carbon nanotube composite. Sens. Actuators B: Chem. 252, 503-510.

Lv, J., Feng, J., Li, S., Wang, Y., Wang, A., Zhang, Q., Chen, J., Feng, J., 2014a. Ionic liquid crystal-assisted synthesis of PtAg nanoflowers on reduced graphene oxide and their enhanced electrocatalytic activity toward oxygen reduction reaction. Electrochim. Acta 133, 407-413.

Lv, J., Li, S., Zheng, J., Wang, A., Chen, J., Feng, J., 2014b. Facile synthesis of reduced graphene oxide supported PtAg nanoflowers and their enhanced electrocatalytic activity. Int. J Hydrogen Energy 39, 3211-3218.

Madhurantakam, S., Selvaraj, S., Nesakumar, N., Sethuraman, S., Rayappan, J.B.B., Krishnan, U.M., 2014. Electrochemical enzymeless detection of superoxide employing

naringin-copper decorated electrodes. Biosens. Bioelectron. 59, 134-139.

Park, S., Chung, T.D., Kim, H.C., 2003. Nonenzymatic glucose detection using mesoporous platinum. Anal. Chem. 75, 3046-3049.

Peng, F., Xu, T., Wu, F., Ma, C., Liu, Y., Li, J., Zhao, B., Mao, C., 2017. Novel biomimetic enzyme for sensitive detection of superoxide anions. Talanta 174, 82-91.

Qiu, H., Li, X., Xu, H., Zhang H., Wang, Y., 2014. Nanoporous metal as a platform for electrochemical and optical sensing. J Mater. Chem. C 2 (46): 9788-9799.

Ren, J., Zhai, M., Cui, M., Li, L., Yu, C., Yu X., Ji, X., 2017. A novel superoxide anion radical nonenzymatic electrochemical sensor based on PtRuCu ternary alloy nanoparticles/graphene composite modified electrode. Nano 12, 1750006 (10pp).

Sadeghian, R.B., Han, J., Ostrovidov, S., Salehi, S., Bahraminejad, B., Ahadian, S., Chen, M., Khademhosseini, A., 2017. Macroporous mesh of nanoporous gold in electrochemical monitoring of superoxide release from skeletal muscle cells. Biosens. Bioelectron. 88, 41-47.

Song, Y., Hao, J., Hu, D., Zeng, M., Li, P., Li, H., Chen, L., Tan, H., Wang, L., 2017. Ratiometric fluorescent detection of superoxide anion with polystyrene@nanoscale coordination polymers. Sens. Actuators B: Chem. 238, 938-944.

Tang, J., Zhu, X., Niu, X., Liu, T., Zhao, H., Lan, M., 2015. Anamperometric superoxide anion radicalbiosensor based on SOD/PtPd-PDARGO modified electrode. Talanta 137, 18-24.

Thandavan, K., Gandhi, S., Sethuraman, S., Rayappan, J.B.B., Krishnan, U.M., 2013. A novel nano-interfaced superoxide biosensor. Sens. Actuators B: Chem. 176, 884-892.

Wang, L., Liu, S., Zheng, Z., Pi, Z., Song, F., Liu, Z., 2015. Rapid assay for testing

superoxide anion radical scavenging activities to natural pigments by ultra-high performance liquid chromatography-diode-array detection method. Anal. Methods 7, 1535-1542.

Wang, M., Ye, C., Bao, S., Xu, M., 2017a. Controlled synthesis of $Mn_3(PO_4)_2$ hollow spheres as biomimetic enzymes for selective detection of superoxide anions released. Microchim. Acta 184, 1177-1184.

Wang, M., Ye, C., Bao, S., Xu, M., Zhang, Y., Wang, L., Ma, X., Guo, J., Li, C., 2017b. Nanostructured cobalt phosphates as excellent biomimetic enzymes to sensitively detect superoxide anions released from living cells. Biosens. Bioelectron. 87, 998-1004.

Wang, M., Ye, C., Bao, S., Zhang, Y., Xu M., Li, Z., 2016. Bimetal-organic-frameworks-derived yolk-shell-structured porous Co_2P/ZnO@PC/CNTs hybrids for highly sensitive non-enzymatic detection of superoxide anion released from living cells. Chem. Commun. 52, 12442-12445.

Wang, Q., Yang, X., Qu, D., 2013. In situ ESR spectro-electrochemical investigation of the superoxide anion radical during the electrochemical O_2 reduction reaction in aprotic electrolyte. Carbon 61, 336-341.

Wang, Q., Zhou, Q., Zhang, Q., Shi, R., Ma, S., Zhao, W., Zhou, M., 2018. Fabrication of novel superoxide anion biosensor based on 3D interface of mussel-inspired Fe_3O_4-$Mn_3(PO_3)_2$@Ni foam. Talanta 179, 145-152.

Wei, H., Shang, T., Wu, T., Liu, G., Ding, L., Liu, X., 2018. Construction of an ultrasensitive non-enzymatic sensor to investigate the dynamic process of superoxide anion release from living cells. Biosens. Bioelectron. 100, 8-15.

Xiao, H., Liu, X., Wu, C., Wu, Y., Li, P., Guo, X., Tang, B., 2017. A new endoplasmic reticulum-targeted two-photon fluorescent probe for imaging of superoxide anion in diabetic mice. Biosens. Bioelectron. 91, 449-455.

Xu, C., Liu, Y., Su, F., Liu, A., Qiu, H., 2011. Nanoporous PtAg and PtCu alloys with hollow ligaments for enhanced electrocatalysis and glucose biosensing. Biosens. Bioelectron. 27, 160-166.

Xu, C., Wang, J., Zhou, J., 2013. Nanoporous PtNi alloy as an electrochemical sensor for ethanol and H_2O_2. Sens. Actuators B: Chem. 182, 408-415.

Yousaf, A.B., Imran, M., Zeb, A., Wen, T., Xie, X., Jiang, Y., Yuan, C., Xu, A., 2016. Single phase PtAg bimetallic alloy nanoparticles highly dispersed on reduced graphene oxide for electrocatalytic application of methanol oxidation reaction. Electrochim. Acta 197, 117-125.

Zhan, D.P., Velmurugan, J., Mirkin, M.V., 2009. Adsorption/desorption of hydrogen on Pt Nanoelectrodes evidence of surface diffusion and spillover. J. Am. Chem. Soc. 131, 14756-14760.

Zheng, F., Luk, S., Kwong T., Yung, K., 2016. Synthesis of hollow PtAg alloy nanospheres with excellent electrocatalytic performances towards methanol and formic acid oxidations. RSC Adv. 6, 44902-44907.

Zhou, J., Luo, Y., Zhu, A., Liu, Y., Zhu Z., Tian, Y., 2011. A reliable and durable approach for real-time determination of cellular superoxide anion based on biomimetic superoxide dismutase stabilized by a zeolite. Analyst 136, 1594-1598.

Zhu, X., Liu, T., Zhao, H., Shi, L., Li, X., Lan, M., 2016. Ultrasensitive detection of superoxide anion released from living cells using a porous Pt-Pd decorated enzymatic

sensor. Biosens. Bioelectron. 79, 449-456.

Zhu, X., Niu, X., Zhao, H., Tang, J., Lan, M., 2015. Immobilization of superoxide dismutase on Pt-Pd/MWCNTs hybrid, modified electrode surface for superoxide anion detection. Biosens. Bioelectron. 67, 79-85.

Figure captions

Fig. 1. SEM (a), TEM (b,c), HRTEM (d), and elemental mapping (e, f, g) images of the PtAg HPNSs.

Fig. 2. (a) XRD patterns of PtAg HPNSs. The standard patterns of pure Pt (JCPDS 04-0802) and Ag (JCPDS 04-0783) are attached for comparison. (b) EDS data of PtAg sample.

Fig. 3. CVs of different electrodes in the PBS solution and PBS+0.01 mM $O_2^{\bullet-}$ solution at 30 mV/s: (a) PtAg HPNSs, (b) commercial Pt/C, and (c) bare GCE.

Fig.4. (a) Amperometric currents of the PtAg HPNSs modified electrode on successive addition of $O_2^{\bullet-}$ into stirring PBS solution at 0.9 V. (b) Linear calibration curve of the current vs. $O_2^{\bullet-}$ concentrations.

Fig. 5. (a) Amperometric responses to the successive addition of 0.5 mM AA, 0.5 mM UA, 0.5 mM DA, 5 mM glucose, 1 mM ethanol and 1.0 μM $O_2^{\bullet-}$ in 0.1 M PBS solution at 0.9 V. (b) Column graph of CV signals of 0.01 mM $O_2^{\bullet-}$ in 0.1 M PBS solution at five different PtAg HPNSs modified electrodes prepared under the same conditions. (c) Amperometric currents of PtAg HPNSs in a stirring PBS solution with 1.0 and 5.0 μM $O_2^{\bullet-}$ for 4000 s at 0.9 V, respectively.

Fig. 6. Current responses of PtAg HPNSs based biosensors in cell suspension under the stimulation of Zymosan: (a) Raw 264.7 cells and (b) HeLa cells.

Figures:

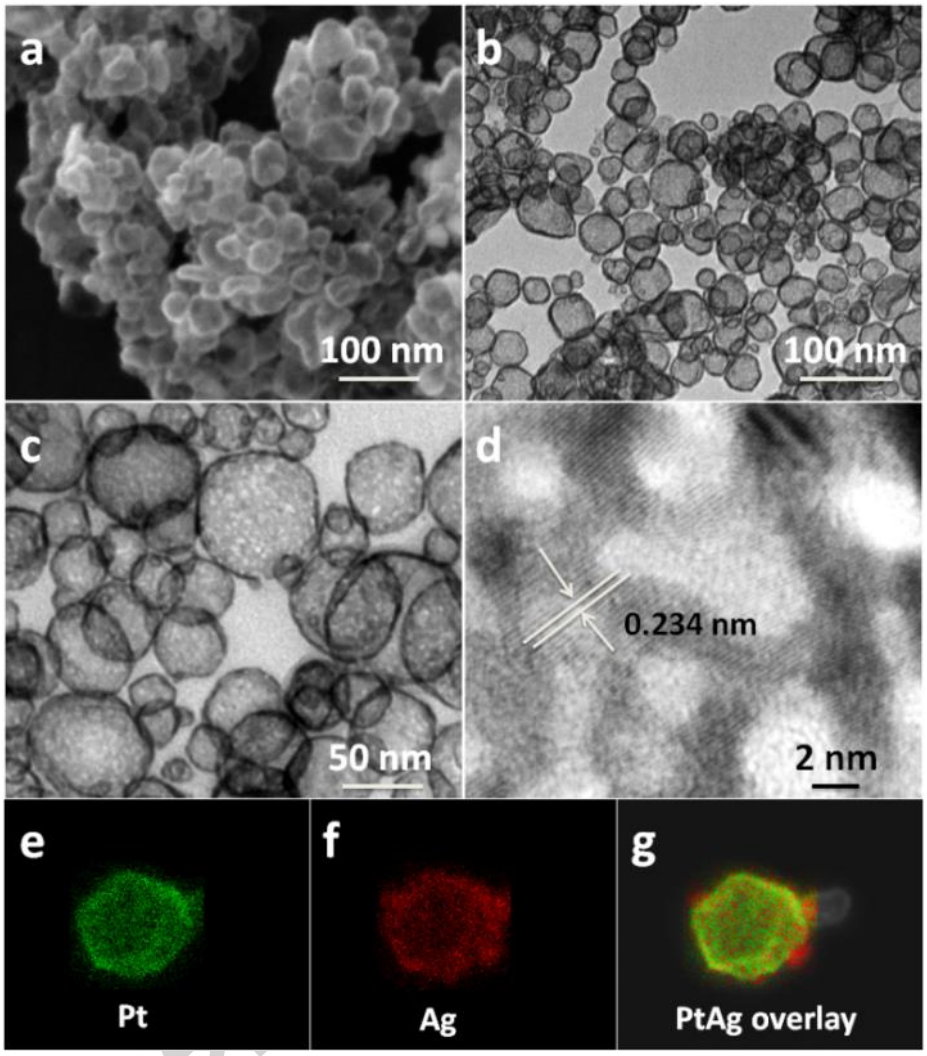

Fig. 1.

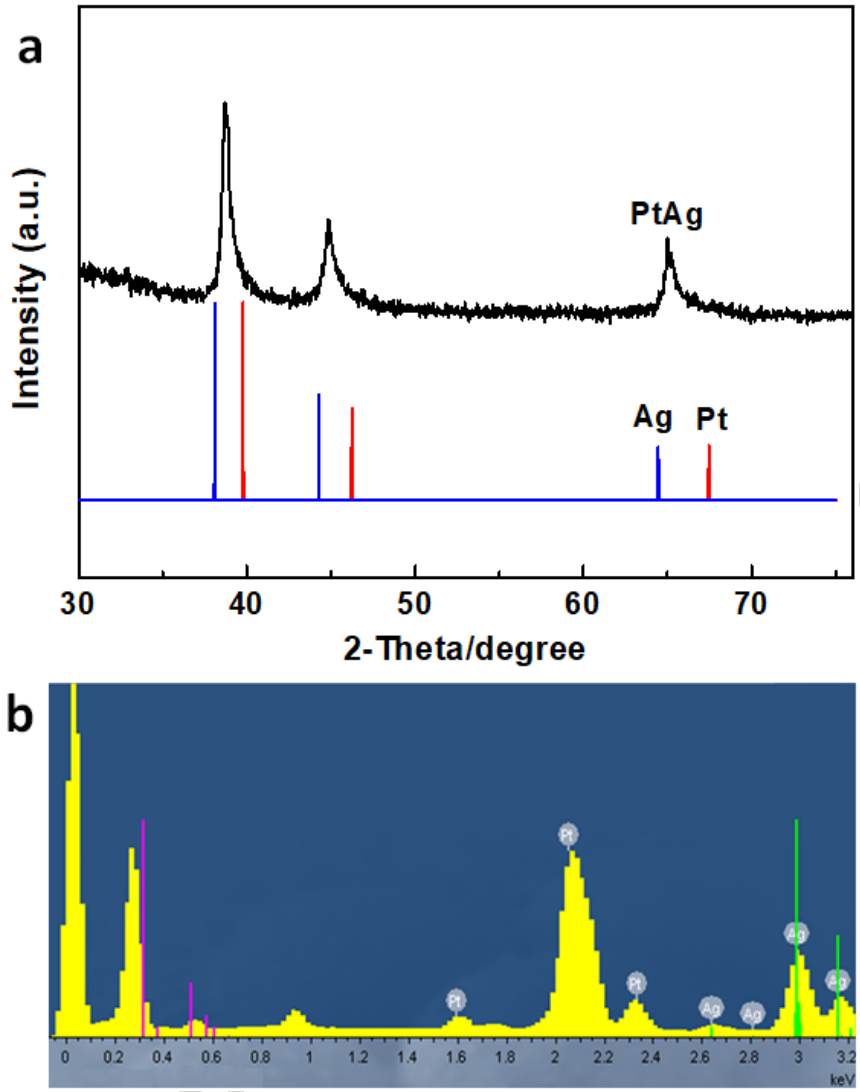

Fig. 2.

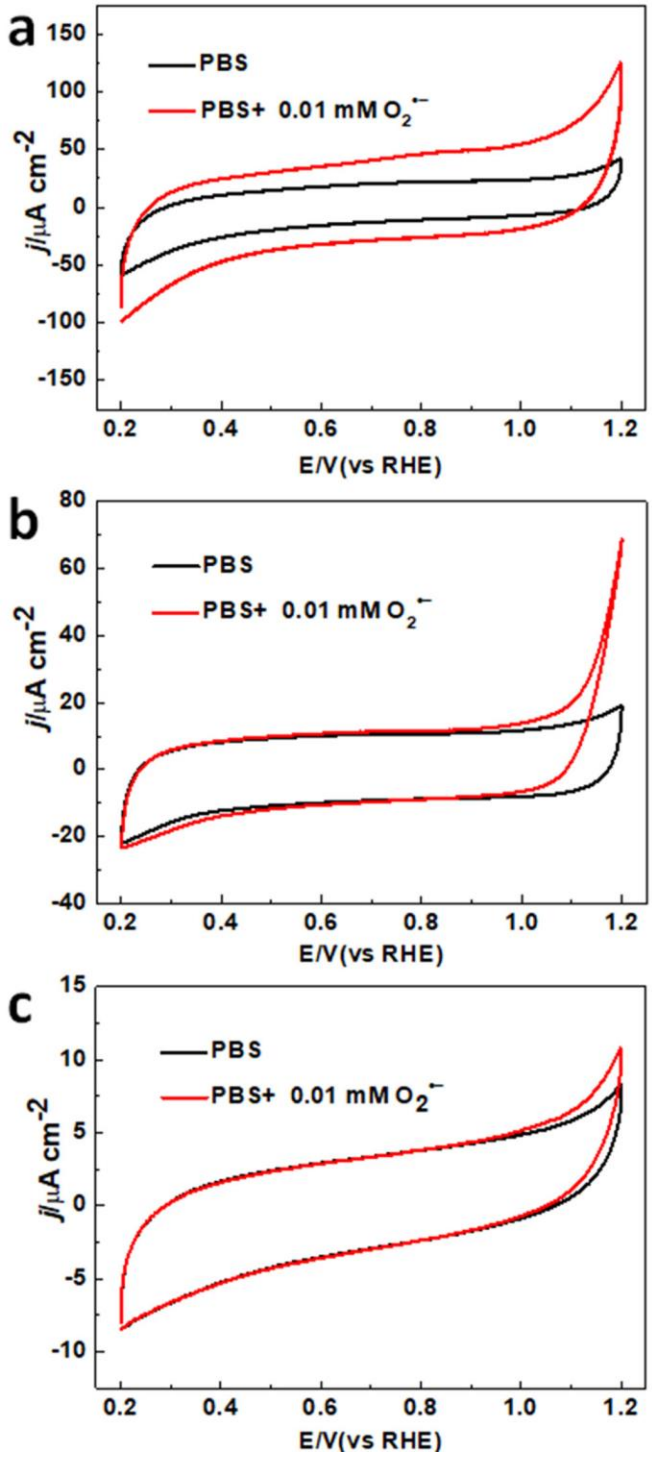
a
PBS
PBS+ 0.01 mM $O_2^{\bullet-}$
j/μA cm^{-2}
E/V(vs RHE)
b
PBS
PBS+ 0.01 mM $O_2^{\bullet-}$
j/μA cm^{-2}
E/V(vs RHE)
c
PBS
PBS+ 0.01 mM $O_2^{\bullet-}$
j/μA cm^{-2}
E/V(vs RHE)

Fig. 3.

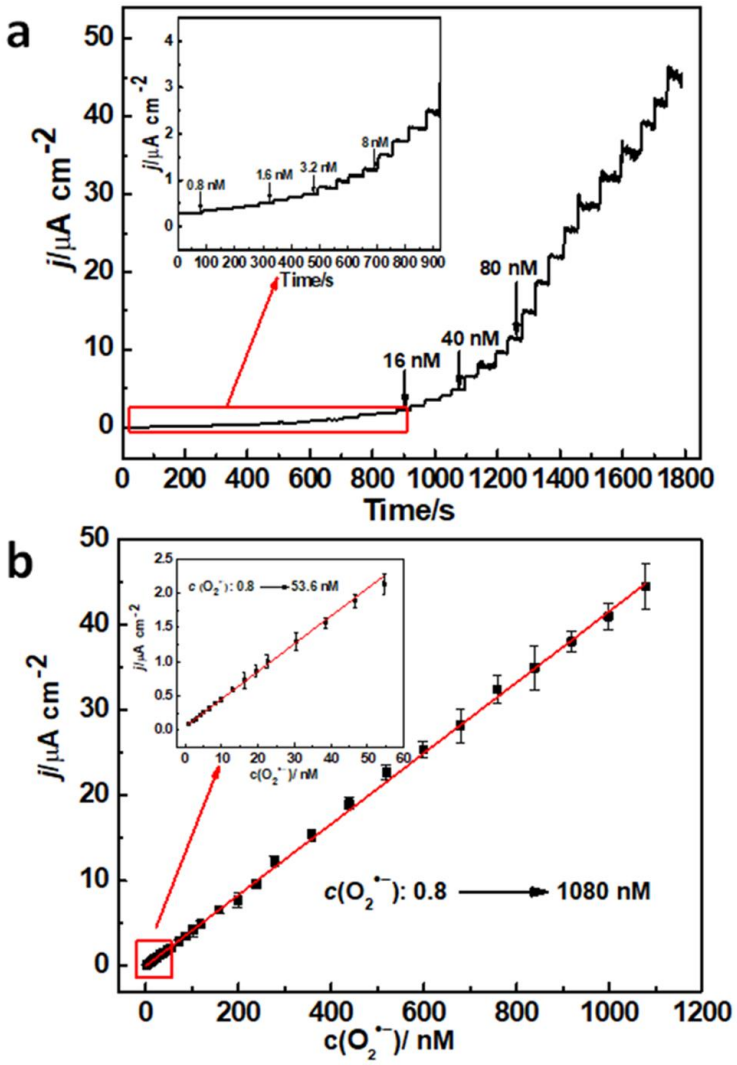
a
j/μA cm-2
Time/s
0.8 nM
1.6 nM
3.2 nM
8 nM
16 nM
40 nM
80 nM
b
j/μA cm-2
c(O2•−)/ nM
c(O2•−): 0.8 → 1080 nM
c(O2•−): 0.8 → 53.6 nM

Fig. 4.

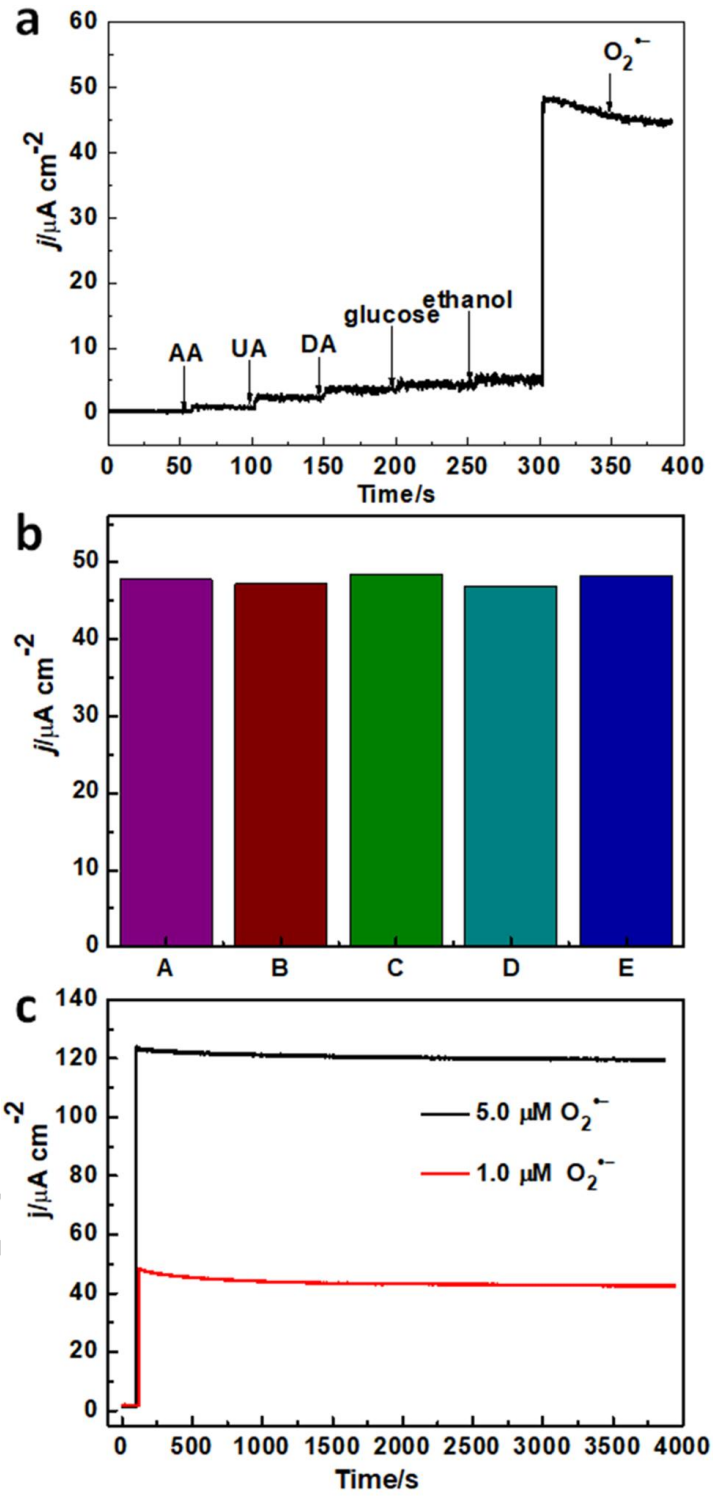
a
j/μA cm-2
Time/s
AA
UA
DA
glucose
ethanol
O2•−
b
j/μA cm-2
A
B
C
D
E
c
j/μA cm-2
Time/s
5.0 μM O2•−
1.0 μM O2•−

Fig. 5.

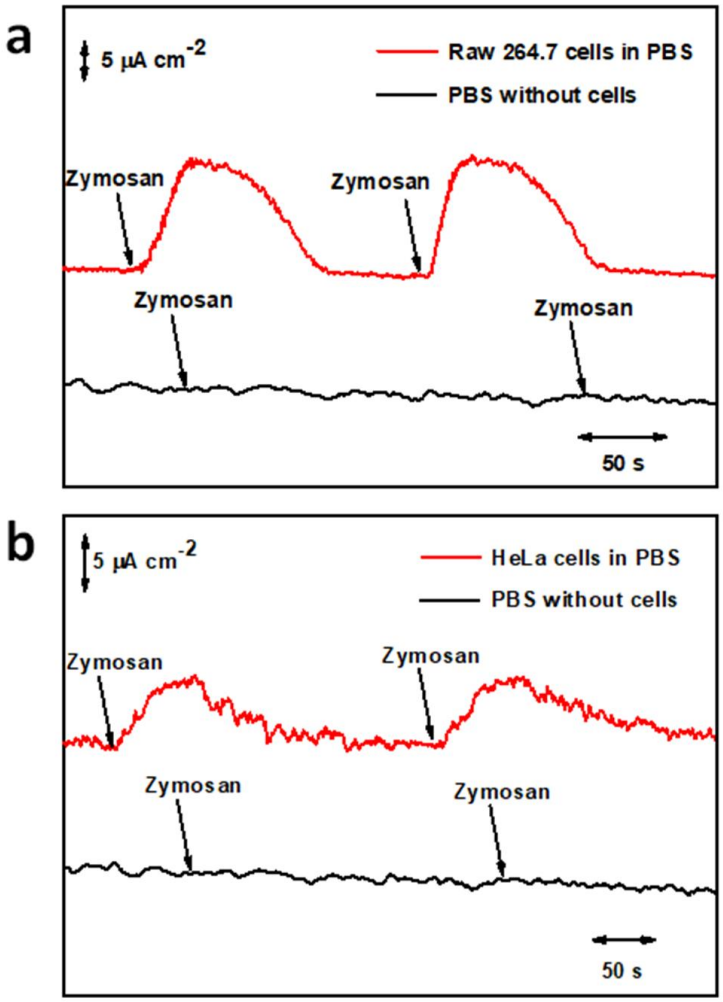

Fig. 6.

Highlights:

1. PtAg nanospheres with porous surface and hollow interiors are easily fabricated.
2. PtAg HPNSs show high electrocatalytic activity and sensing ability toward $O_2^{\bullet-}$.

3. PtAg HPNSs constructed sensor shows a wide linear range and low detection limit.
4. The sensor achieves real time detection of $O_2^{\bullet-}$ released from living cells.